Available online at www.sciencedirect.com
SCIENCE DIRECT®
Journal of Solid State Chemistry 179 (2006) 632–645
JOURNAL OF SOLID STATE CHEMISTRY
www.elsevier.com/locate/jssc

Hole doping into Co-12*s*2 copper oxides with *s* fluorite-structured layers between CuO_2 planes

H. Fjellvåg[a,b], Y. Morita[a], T. Nagai[c], J.-M. Lee[d], J.-M. Chen[d], R.-S. Liu[e], B.C. Hauback[f], V.P.S. Awana[a,g], Y. Matsui[c], H. Yamauchi[a], M. Karppinen[a,*]

[a]*Materials and Structures Laboratory, Tokyo Institute of Technology, 4259 Nagatsuta, Midori-ku, Yokohama 226-8503, Japan*
[b]*Centre for Materials Science and Nanotechnology, University of Oslo, N-0315 Oslo, Norway*
[c]*National Institute for Materials Science, 1-1 Namiki, Tsukuba, Ibaraki 305-0044, Japan*
[d]*National Synchrotron Radiation Research Center, Hsinchu, Taiwan, ROC*
[e]*Department of Chemistry, National Taiwan University, Taipei, Taiwan, ROC*
[f]*Institute for Energy Technology, N-2027 Kjeller, Norway*
[g]*National Physical Laboratory, Krishnan Matg, New Delhi 12, India*

Received 19 August 2005; received in revised form 9 November 2005; accepted 12 November 2005
Available online 20 January 2006

Abstract

In this work, the first three members ($s = 1, 2, 3$) of the Co-12*s*2 homologous series of multi-layered copper oxides are gradually doped with holes through high-pressure oxygenation (HPO). The phases differ from each other only by thickness of the fluorite-structured layer block, (Ce,Y,Ca)–$[O_2$–(Ce,Y)$]_{s-1}$, between two identical CuO_2 planes. High-resolution transmission-electron microscopy (HRTEM) and electron diffraction (ED) analyses together with both synchrotron X-ray and neutron powder diffraction data, reveal that as a consequence of HPO the charge-reservoir CoO_4-tetrahedra chains get broken and the lattice symmetry of the Co-12*s*2 phases changes from orthorhombic to tetragonal. Oxygen contents are analyzed for the samples with wet-chemical and thermogravimetric techniques. The valence state of copper in the CuO_2 plane is determined from Cu *L*-edge X-ray absorption near-edge structure (XANES) spectra to be compared with the values estimated through bond-valence-sum (BVS) calculations from the crystal structure data. The positive charge induced by oxygen loading (or aliovalent Ca^{II}-for-Y^{III} substitution in $CoSr_2YCu_2O_{7+\delta}$) is found not to be completely accommodated in the CuO_2 planes but be rather effectively trapped at the charge-reservoir Co atoms. Superconductivity appears in the Co-1212 ($CoSr_2YCu_2O_{7+\delta}$) samples with the copper valence of 2.13 or higher, whereas in the Co-1222 ($CoSr_2(Ce_{0.25}Y_{0.75})_2Cu_2O_{9+\delta}$) and Co-1232 ($CoSr_2(Ce_{0.67}Y_{0.33})_3Cu_2O_{11+\delta}$) samples Cu valence does not increase high enough to induce superconductivity.

Keywords: Multi-layered copper oxides; Fluorite-structured layers; Co-12*s*2 homologous series; Crystal structure; Oxygen content; Hole-doping; Cu valence; XANES spectroscopy; Superconductivity

1. Introduction

To date more than hundred different copper-oxide phases that show high-T_c superconductivity in their hole-doped CuO_2 plane(s) have been discovered. The high-T_c superconductor characteristically has a layered crystal structure in which the superconductive CuO_2 plane(s) alternate with non-stoichiometric and non-superconductive layers, the latter playing a dual role of a "spacing provider" and a "redox controller" for the former. There also exist a large number of related multi-layered copper-oxide phases for which superconductivity has not been observed yet. In order to comprehend the occurrence of high-T_c superconductivity in many of the complex copper oxide phases it is also essentially important to search for routes that might "superconductorize" some of the relevant candidate phases and then rationalize the reasons for the occurrence/absence of superconductivity in such phases. A majority of the not-yet-superconductorized but potential high-T_c superconductors are phases that belong to so-called "Category-B" [1,2]: they contain an additional fluorite-structured layer-block

*Corresponding author. Fax: +81 45 924 5365.
E-mail address: karppinen@msl.titech.ac.jp (M. Karppinen).

0022-4596/$ - see front matter © 2005 Elsevier Inc. All rights reserved.
doi:10.1016/j.jssc.2005.11.025

of (Ce,*R*)–[O_2–(Ce,*R*)]$_{s-1}$ (*R* = rare earth element; valence states of Ce^{IV} and R^{III} are assumed) between two CuO_2 planes (i.e., the basal planes of corner-linked CuO_5 square-pyramid layers). The Category-B phase obeys the general formula of $M_mA_2(Ce,R)_sCu_2O_{m+4+2s\pm\delta}$ (*M* = Cu, Pb, Tl, Hg, etc.; *A* = Ba, Sr, etc.) expressed in short as *M*-*m*2*s*2 [2].

We recently synthesized samples of a three-fluorite-layer (*s* = 3) phase, Co-1232 of the composition of $CoSr_2(Ce_{0.67}Y_{0.33})_3Cu_2O_{11+\delta}$ [3,4]. Together with two previously known phases, Co-1212 ($CoSr_2YCu_2O_{7+\delta}$) [5–7] and Co-1222 ($CoSr_2(Ce_{0.4}Nd_{0.6})_2Cu_2O_{9+\delta}$) [8,9], the *s* = 3 phase forms a homologous series of Co-12*s*2 of Category-B (Fig. 1). In these phases two adjacent CuO_2 planes are separated from each other by a single *R*-cation layer for *s* = 1, a "double-fluorite-layer" block of (Ce,*R*)–O_2–(Ce,*R*) for *s* = 2, and a "triple-fluorite-layer" block of (Ce,*R*)–O_2–(Ce,*R*)–O_2–(Ce,*R*) for *s* = 3. It should be noted that the first member of the series, i.e., Co-1212, is isostructural with the $CuBa_2RCu_2O_{7-\delta}$ phase (Cu-1212 or "*R*-123") in terms of the layer sequence, *A*O-$MO_{1\pm\delta}$-*A*O-CuO_2–*R*–CuO_2. When synthesized by solid-state reaction in air, the single-phase samples of the three Co-12*s*2 phases are all essentially stoichiometric in terms of oxygen content, i.e., $\delta \approx 0$ for the $CoO_{1+\delta}$ "charge reservoir" [3]. Moreover it is known that, at $\delta = 0$ the charge reservoir of all the three Co-12*s*2 phases consists of zigzag chains of corner-linked CoO_4 tetrahedra that run diagonally relative to the perovskite base. Precise electron diffraction (ED) and high-resolution transmission-electron microscopy (HRTEM) studies have furthermore revealed a superstructure originating from a regular alternation of two zigzag chains that are mirror images of each other [4,6].

As-air-synthesized samples of Co-12*s*2 do not show superconductivity [3–9]. However, by taking advantage of a high-pressure oxygenation (HPO) technique we recently succeeded in making $CoSr_2(Y,Ca)Cu_2O_{7+\delta}$ samples of the Co-1212 phase superconductive [10]. At the same time, it was found that aliovalent Ca^{II}-for-Y^{III} substitution alone could not induce superconductivity. In the present work the HPO technique was first employed to introduce excess oxygen into the higher members of the Co-12*s*2 homologous series, i.e., Co-1222 and Co-1232. It turned out that even though excess oxygen was successfully loaded into these phases, it did not induce superconductivity. Therefore, the next goal was to elucidate reasons for this. Additionally, searched were possible reasons why

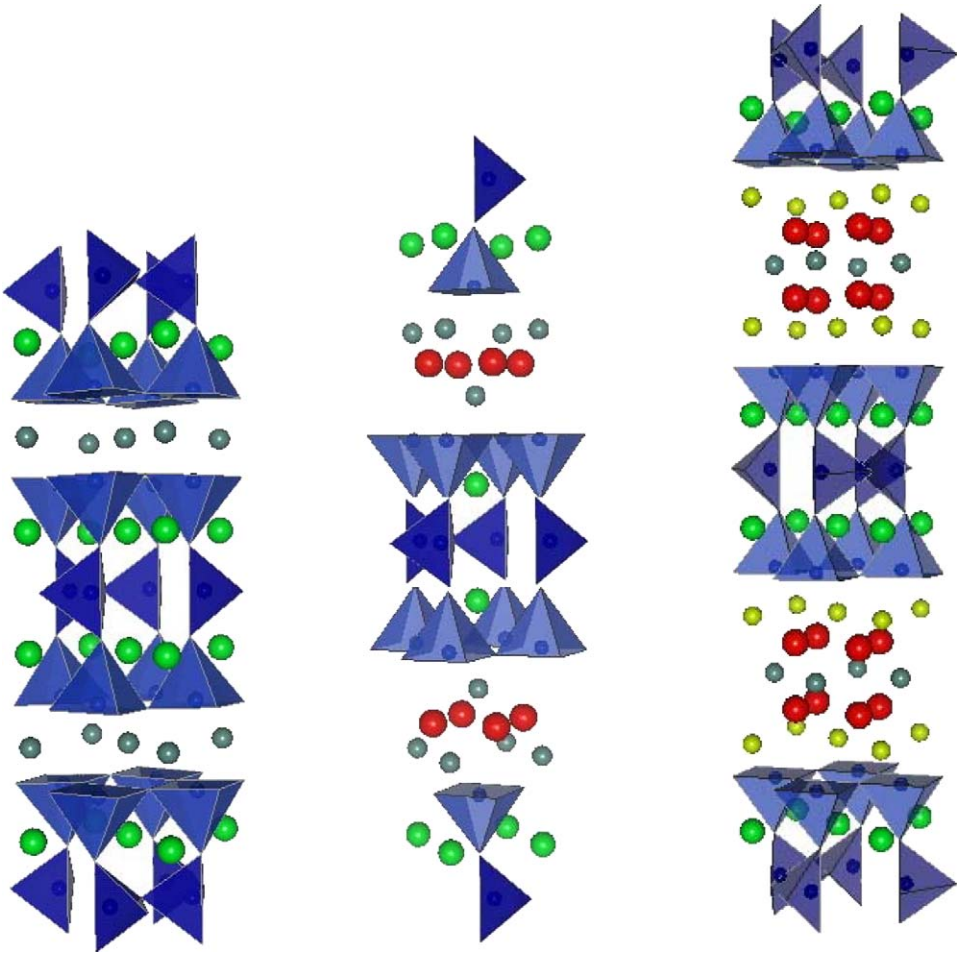

Fig. 1. Crystal structures of the first three members of the Co-12*s*2 homologous series.

oxidation of Co-1212 by means of aliovalent Ca^{II}-for-Y^{III} substitution does not induce superconductivity while that by means of increase in the oxygen content through HPO does. The changes in oxygen content, CuO_2-plane hole concentration and average and local atomic structures were probed by complementary experimental techniques, i.e., iodometric titration, thermogravimetry (TG), X-ray absorption near-edge structure (XANES) spectroscopy, synchrotron X-ray diffraction (SXRD) and neutron powder diffraction (NPD) as well as HRTEM and ED.

2. Experimental

2.1. Sample synthesis

Powder samples of $CoSr_2(Y_{1-x}Ca_x)Cu_2O_{7+\delta}$ (Co-1212; $0 \leqslant x \leqslant 0.4$), $CoSr_2(Ce_{0.25}Y_{0.75})_2Cu_2O_{9+\delta}$ (Co-1222) and $CoSr_2(Ce_{0.67}Y_{0.33})_3Cu_2O_{11+\delta}$ (Co-1232) were prepared by means of conventional solid-state reaction synthesis. The starting materials, Co_3O_4, $SrCO_3$, CeO_2, Y_2O_3 and CuO, were mixed to appropriate ratios [11]. The powder mixtures were calcined at 950 °C for 24 h and sintered at either 1000 °C (24 h) or 1050 °C (3×24 h) to obtain Co-1212 or Co-1222/Co-1232 samples, respectively. All the heat treatments were carried out in air. For subsequent HPO a portion of the as-air-synthesized sample was first mixed with 12.5–150 mol% of Ag_2O_2 (i.e., 0.125–1.5 mol for 1 mol of the Co-12*s*2 phase) for excess-oxygen source and then treated for 30 min at 5 GPa and 500 °C in a cubic-anvil-type ultra-high-pressure apparatus. Under these conditions Ag_2O_2 efficiently releases oxygen upon decomposing to Ag_2O and/or metallic Ag. Powder X-ray diffraction measurements were performed to check the phase purity and to determine the lattice parameters for all the samples. The following naming scheme is used: AS for as-air-synthesized samples; HPO-*y* for high-pressure-oxygenated samples with *y* mol% Ag_2O_2.

2.2. Oxygen content analyses

For AS samples, the overall oxidation state of the high-valent Cu and Co species, i.e., $Cu^{II/III}$ and $Co^{III/IV}$, and thereby the oxygen content, were precisely determined by iodometric titrations. Experimental details were as described in Refs. [3,12]. It was not considered feasible to perform wet-chemical analysis for the HPO samples due to the presence of silver oxide(s) in not-well-defined ratios. Instead, the amount of "excess" or removable oxygen was estimated on the basis of TG (MAC Science: TG/DTA 2000 S) runs carried out for a specimen of ~10 mg in flowing N_2 gas at a rate of 1 °C/min up to 500 °C.

2.3. Determination of Cu valence

Since iodometric titration determines only the total oxidation power of high-valent Cu and Co species [12], Cu $L_{2,3}$-edge XANES spectroscopy was utilized to selectively determine the valence of copper, V(Cu). X-ray absorption data were collected at the 6-m HSGM beam-line at NSRRC in Hsinchu, Taiwan. All spectra were recorded at room temperature in fluorescence-yield mode using a micro-channel-plate detector system; details were as those given elsewhere [13]. The photon energies were calibrated against the Cu L_3 white line of CuO at 931.2 eV with an accuracy of 0.1 eV. The monochromator resolution was set to ~0.45 eV. The spectral data were corrected for the energy-dependent incident photon intensity. Spectral features were analyzed as done previously [14]. The main peak seen in the Cu L_3-edge area at 931.1–931.2 eV and its high-energy shoulder at 932.5–932.8 eV were fitted with Gaussian functions after approximating the background to a straight line. The intensity of the main peak is proportional to the amount of divalent copper [$I(Cu^{II})$], whereas that of the shoulder reflects the amount of trivalent copper [$I(Cu^{III})$] [15,16]. Thus, V(Cu) was estimated at $V(Cu) = 2 + I(Cu^{III})/[I(Cu^{II}) + I(Cu^{III})]$. Owing to the large number of samples studied, we carried out corrections for the self-absorption effect for representative samples only. It was found that in general the corrected V(Cu) values are slightly ($\leqslant 0.03$) smaller than the non-corrected values. In the following, we systematically refer to non-corrected V(Cu) values, which hence may somewhat overestimate the real Cu valence values, but should within the sample series studied be highly reliable in terms of detecting relative changes/differences in the valence state of copper.

2.4. Crystal structure analyses

The AS and HPO-25 samples of $CoSr_2(Y_{0.6}Ca_{0.4})Cu_2O_{7+\delta}$ (Co-1212) were characterized structurally by means of HRTEM and ED using an ultra-high-voltage transmission electron microscope (Hitachi: H-1500) operated at an accelerating voltage of 820 kv. The specimen was prepared by crushing a portion of the sample into fine fragments, which were ultrasonically dispersed in CCl_4 and transferred to carbon microgrids. The same samples together with the AS samples of $CoSr_2YCu_2O_{7+\delta}$ (Co-1212) and $CoSr_2(Ce_{0.67}Y_{0.33})_3Cu_2O_{11+\delta}$ (Co-1232) were studied by NPD at 8 and/or 298 K. The NPD data were collected at the JEEP-II reactor at Kjeller, Norway, using the high-resolution two-axis powder diffractometer, PUS. The amount of the HPO-25 $CoSr_2(Y_{0.6}Ca_{0.4})Cu_2O_{7+\delta}$ sample was just ~550 mg, whereas ~3 g otherwise. A cylindrical vanadium sample holder, sealed with an indium washer, was used. Monochromatized neutrons of wavelength 1.5554 Å were obtained from a Ge(511) monochromator. Data were collected in the 2θ range of 10–130° (in 2θ steps of 0.05°) by means of two detector units, each containing a vertical stack of seven position-sensitive ^{3}He detectors and covering a range of 20° in 2θ. A Displex cooling system was used for the low-temperature measurements. Additionally SXRD data were collected at room temperature at SPring-8, Japan (beamline: Bl02b2) using radiation with wavelength of 0.500981 Å. For these

Table 1
Relevant parameters of the data collection and Rietveld refinements of the NPD (N) and SXRD (S) data

	$CoSr_2(Y_{1-x}Ca_x)Cu_2O_{7+\delta}$					$CoSr_2(Ce_{0.67}Y_{0.33})_3Cu_2O_{11+\delta}$	
	AS ($x = 0.0$) 298 K	AS ($x = 0.4$) 8 K	AS ($x = 0.4$) 298 K	HPO-25 ($x = 0.4$) 298 K	HPO-25 ($x = 0.4$) 8 K	AS 298 K	AS 8 K
Pattern range 2θ (°)	2–50 (S)		2–50 (S)	2–50 (S)			
	10–130 (N)	10–130 (N)	10–130 (N)		10–130 (N)	10–130 (N)	10–130 (N)
Step size $\Delta 2\theta$ (°)	0.01(S)		0.01 (S)	0.01 (S)			
	0.05 (N)	0.05 (N)	0.05 (N)		0.05 (N)	0.05 (N)	0.05 (N)
Wavelength (Å)	0.50098 (S)		0.50098 (S)	0.50098 (S)			
	1.5554 (N)	1.5554 (N)	1.5554 (N)		1.5554 (N)	1.5554 (N)	1.5554 (N)
No. observations	4780 (S)		4780 (S)	4779 (S)			
	2399 (N)	2399 (N)	2399 (N)		2338 (N)	2399 (N)	2399 (N)
No. reflections	1002 (S)		1002 (S)	353 (S)			
	330 (N)	324 (N)	330 (N)		129 (N)	496 (N)	492 (N)
No. refined params.	43	21	43	29	30	37	37
R_{wp}	0.055 (S)		0.079 (S)	0.045 (S)			
	0.074 (N)	0.057 (N)	0.057 (N)		0.059 (N)	0.074 (N)	0.062 (N)
R_F^2	0.089 (S)		0.109 (S)	0.109 (S)			
	0.087 (N)	0.069 (N)	0.079 (N)		0.114 (N)	0.082 (N)	0.074 (N)

experiments the sample was crushed into fine powder and sealed in a quartz capillary of 0.1 mm diameter.

The crystal structure refinements were made using the GSAS [17] software, whereas the Fullprof [18] software was used to include description of magnetic order at 8 K. Details of the measurement and refinement parameters are given in Table 1. Combined refinements using both NPD and SXRD data were performed. The background was in general described with 9–12 term cosine Fourier series polynomials. Regions with scattering from Al of the cryostat (NPD) were excluded. The NPD data were fitted using a Gaussian peak shape function, SXRD data by basically a Lorentzian peak shape (profile function #3; GSAS). The oxygen contents for HPO samples were estimated from refined oxygen [O(1), O(2)] occupation numbers, Table 2.

To facilitate comparison with the XANES data, we used the refined atomic positions (at room temperature) to estimate the valence value of copper on the basis of bond-valence-sum (BVS) calculation. Such estimate, BVS(Cu), was calculated from the derived bond lengths between Cu and the apical O atom, O_{api}, plus the four in-plane O atoms along the *a*- and *b*-axis, $O_{a/b}$, using 1.679 as the "unit valence bond-length" [19].

2.5. Magnetic/superconductivity characterization

Magnetization under a magnetic field of 10 Oe was measured for all the samples down to 5 K in both field-cooled (FC) and zero-field-cooled (ZFC) modes using a superconducting-quantum-interference-device (SQUID) magnetometer (Quantum Design: MPMS-XL). For the superconductive samples T_c is determined at the onset temperature of the diamagnetic signal.

3. Results and discussions

3.1. Sample quality

From XRD patterns (not shown here) for the HPO samples it was revealed that upon high-pressure treatment the excess-oxygen source Ag_2O_2 decomposes completely to Ag as long as its amount is low (12.5–25 mol%). For samples with the higher Ag_2O_2 contents peaks due to the intermediate-decomposition product Ag_2O were seen in the diffraction patterns together with those of Ag. Therefore the actual oxygen pressure in the high-pressure sample cell is most likely lower than what one might expect on the basis of complete decomposition of Ag_2O_2 to Ag. On the other hand, except for the decomposition residue(s) of Ag_2O_2 in the HPO samples, the present samples were found to be of a single Co-12*s*2 phase within the detection limits of laboratory XRD up to 75 mol% Ag_2O_2 addition. For the samples with the amount of Ag_2O_2 exceeding 75 mol% small unidentified diffraction peaks appeared. Moreover, for the AS sample of the Co-1232 phase a slight impurity of CeO_2 ($a = 5.4040$ Å at 8 K) was revealed by both SXRD and NPD.

Intermixing between the cobalt and copper sublattices was suggested in the original work of Huang et al. [5] on their Ca-for-Y substituted samples of the Co-1212 phase. The possibility of Co/Cu intermixing was taken into account in the present study as well. Owing to the large difference in the neutron scattering length between Co and Cu, intermixing of the order of 10% would increase the *R* factors significantly (though yet a reasonable fit would be obtained owing to the many adjustable structure parameters). Such fittings were tried, but the present data gave no indication of Co/Cu intermixing in any of the samples

Table 2
Atomic coordinates for the $CoSr_2(Y_{1-x}Ca_x)Cu_2O_{7+\delta}$ samples as derived from separate or combined (298 K) Rietveld refinement of NPD and SXRD data

	AS, $x = 0.0$ 298 K	AS, $x = 0.4$ 298 K	AS, $x = 0.4$ 8 K	HPO, $x = 0.4$ 8 K
Space group	*Imam*	*Imam*	*Imam*	*P4/mmm*
Z	4	4	4	1
a (Å)	5.41517(10)	5.40200(12)	5.38983(16)	3.8157(2)
b (Å)	5.46006(10)	5.44701(12)	5.43663(16)	—
c (Å)	22.7699(5)	22.7989(5)	22.7201(6)	11.272(1)
V (Å^3)	673.240(23)	670.851(25)	665.754(33)	164.12(2)
Y/Ca				
x	0	0	0	0.5
y	0	0	0	0.5
z	0	0	0	0.5
Uiso	0.30(6)	0.17(6)	0.01(6)	0.2(2)
Sr				
x	0	0	0	0.5
y	0.0073(7)	0.0091(6)	0.0072(7)	0.5
z	0.3482(1)	0.3489(1)	0.3495(1)	0.1879(5)
Uiso	0.93(5)	0.95(5)	0.61(5)	1.3(1)
Co				
x	0	0	0	0
y	0.5548(11)	0.5545(15)	0.5563(21)	0
z	0.25	0.25	0.25	0
Uiso	1.18(16)	1.40(18)	2.40(18)	0.9(1)
Cu				
x	0.5	0.5	0.5	0
y	0.0016(7)	0.0006(7)	0.0005(7)	0
z	0.4265(1)	0.4268(1)	0.4271(1)	0.3553(5)
Uiso	0.39(4)	0.79(4)	0.52(4)	0.9(1)
O(1)				
x	0.396(1)	0.397(1)	0.391(1)	0.5
y	0.612(1)	0.620(1)	0.620(1)	0.830(9)
z	0.25	0.25	0.25	0.009(4)
Uiso	0.79(5)	0.97(5)	0.71(3)	1.1(1)
n	0.5	0.5	0.5	0.109(9)
O(2)				
x	0.25	0.25	0.25	0.5
y	0.75	0.75	0.75	0
z	0.4332(2)	0.4325(2)	0.4321(2)	0
Uiso	0.79(5)	0.97(5)	0.71(3)	1.1(1)
n				0.14(3)
O(3)				
x	0.75	0.75	0.75	0
y	0.25	0.25	0.25	0
z	0.4381(2)	0.4362(2)	0.4366(2)	0.1621(6)
Uiso	0.79(5)	0.97(5)	0.71(3)	1.1(1)
O(4)				
x	0	0	0	0.5
y	0.4671(5)	0.4667(5)	0.4667(5)	0
z	0.3236(2)	0.3239(2)	0.3248(1)	0.3668(4)
Uiso	0.79(5)	0.97(5)	0.71(3)	1.1(1)

Refined composition for nominal $x = 0.40$ is $x = 0.35$, see text. *Calculated* standard deviations are in parentheses. Refined oxygen occupation numbers given for disordered oxygen atoms [O(1) in 8*t*; $\frac{1}{2}$, y,z ; O(2) in 2*f*; $\frac{1}{2}$, 0, 0] in HPO-40. O(1) site half filled in AS Co-1212; see text.

studied. On the other hand, for the $CoSr_2(Y_{1-x}Ca_x)Cu_2O_{7+\delta}$ (Co-1212) samples with the nominal Ca content at $x = 0.40$ negative displacement factors were obtained for the Co and (Y,Ca) atoms unless the magnitude of x was adjusted in refinements to 0.35.

The Co-1232 phase was obtained in single-phase form within the narrow Ce:Y stoichiometry range about 2:1 only, i.e., $CoSr_2(Ce_{0.67}Y_{0.33})_3Cu_2O_{11+\delta}$. From this 2:1 ratio for the two cation constituents that occupy the two non-equivalent sites of the three cation layers within the fluorite-structured block one might suspect that these cations are ordered. However, refinements of the combined data from SXRD and NPD confirmed that Ce and Y are disordered inside the triple-fluorite-layer block.

3.2. Oxygen content

Precise oxygen-content determination by means of iodometric titrations confirmed that the AS samples of the three Co-12*s*2 phases are all oxygen-stoichiometric within ± 0.03 oxygen atoms per formula unit. Moreover it was found that the oxygen content in these samples remained unaffected against normal-pressure annealing in both oxygenative (pure O_2) and inert (N_2) atmospheres [3]. It thus seems that the AS samples, not only in overall but also within each of the individual structural layers, are oxygen stoichiometric. This conclusion is supported by the NPD data for the AS sample of the Co-1232 phase, indicating no oxygen vacancies for any of the layers/blocks. Provided that the fluorite-structured (Ce,Y)–$[O_2$–(Ce,Y)$]_{s-1}$ blocks do not contain oxygen vacancies, the excess oxygen loaded through HPO is to be located exclusively in the $CoO_{1+\delta}$ charge reservoir.

Wet-chemical oxygen-content determination was not possible for the HPO samples due to the presence of Ag, Ag_2O and/or Ag_2O_2. Instead, we utilize here lattice parameter and TG data for discussing the oxygen contents in these samples. In Fig. 2, the c lattice parameters for the Co-12*s*2 phases are plotted against the amount of Ag_2O_2 used in the HPO. For all the three phases, $CoSr_2YCu_2O_{7+\delta}$ (Co-1212), $CoSr_2(Ce_{0.25}Y_{0.75})_2Cu_2O_{9+\delta}$ (Co-1222) and $CoSr_2(Ce_{0.67}Y_{0.33})_3Cu_2O_{11+\delta}$ (Co-1232), oxygen loading shortens the c parameter. However, the c parameter decreases monotonically only up to 25–50 mol% and then saturates for larger Ag_2O_2 amounts. We believe that the oxygen contents follow the same trend, increasing with increasing Ag_2O_2 amount up to a certain level beyond which only minor changes in oxygen content would occur. Moreover, Fig. 2 reveals that the shrinkage in the c parameter is of the same magnitude for all the three Co-12*s*2 phases, i.e., 0.28 Å ($s = 1$), 0.27 Å ($s = 2$) and 0.28 Å ($s = 3$). This suggests that the maximum amount of oxygen that can be incorporated into the $CoO_{1+\delta}$ charge reservoir is essentially the same for the three phases.

Thermogravimetric experiments performed for the HPO samples in N_2 gas flow with a heating rate of 1 °C/min up to 500 °C ended up with essentially parallel conclusions.

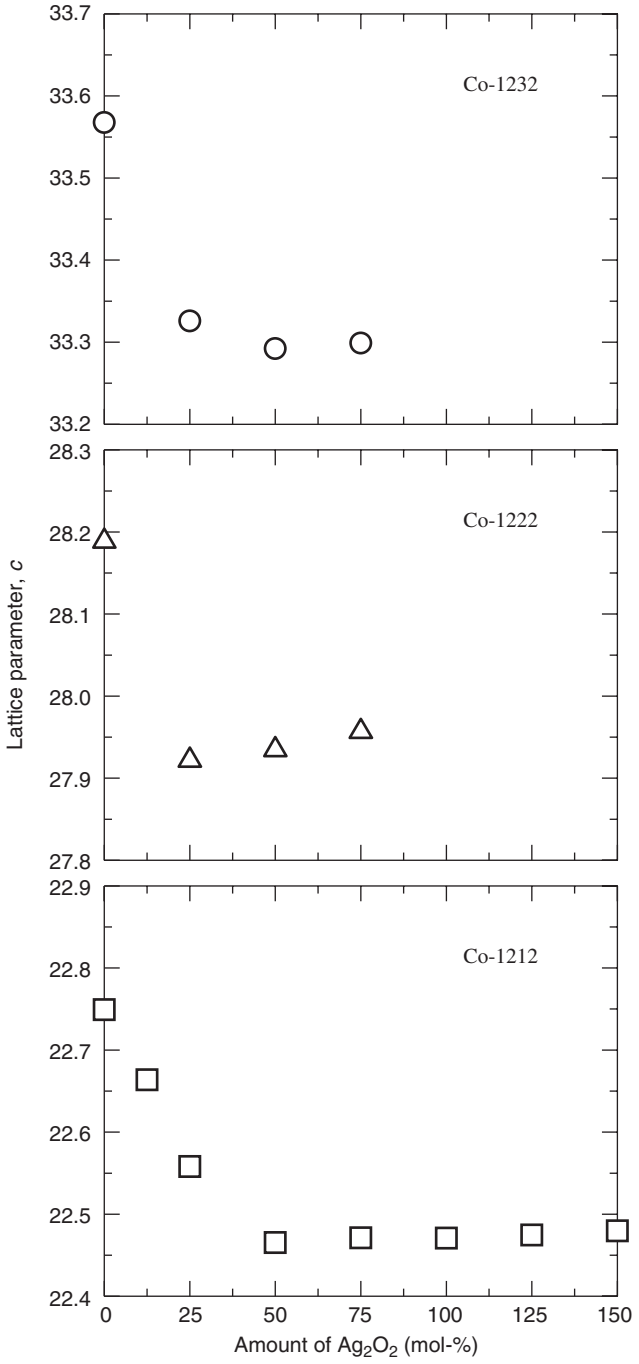

Fig. 2. Lattice parameter, c, plotted against the amount of Ag_2O_2 used for HPO for the three phases of $CoSr_2YCu_2O_{7+\delta}$ (Co-1212), $CoSr_2(Ce_{0.25}Y_{0.75})_2Cu_2O_{9+\delta}$ (Co-1222) and $CoSr_2(Ce_{0.67}Y_{0.33})_3Cu_2O_{11+\delta}$ (Co-1232).

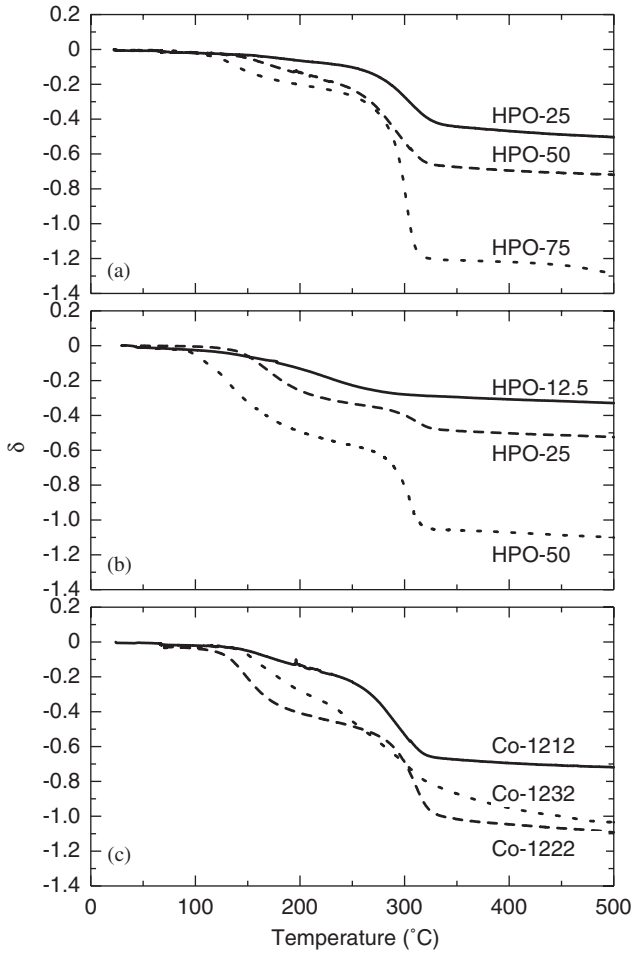

Fig. 3. TG curves for the N_2 annealing of the HPO samples of (a) $CoSr_2YCu_2O_{7+\delta}$ and (b) $CoSr_2(Y_{0.60}Ca_{0.40})Cu_2O_{7+\delta}$ prepared using different amounts of Ag_2O_2, and (c) the HPO-50 samples of $CoSr_2YCu_2O_{7+\delta}$ (Co-1212), $CoSr_2(Ce_{0.25}Y_{0.75})_2Cu_2O_{9+\delta}$ (Co-1222) and $CoSr_2(Ce_{0.67}Y_{0.33})_3Cu_2O_{11+\delta}$ (Co-1232). The first/second weight-loss step is due to oxygen evolution from the Co-12s2 phase/decomposition of leftover Ag_2O.

Fig. 3 shows representative TG curves. Two distinct weight-loss steps are seen. Obviously, only the first with the onset about 150 °C is due to oxygen loss from the Co-12s2 phase. The second weight-loss step about 300 °C reflects thermal decomposition of the left-over Ag_2O [14]. This step is not seen for HPO-12.5 samples, and is just faintly distinguishable even for HPO-25 samples, whereas it becomes prominent for samples with the initial amount of Ag_2O_2 exceeding 50 mol%. Since the two weight-loss steps are well separated, the amount of oxygen removable from the HPO Cu-12s2 phases can be determined. We assume that this corresponds to the amount of oxygen that was incorporated upon HPO treatment into the original AS phases, and hence represents δ for these samples. From Figs. 3(a) (for $CoSr_2YCu_2O_{7+\delta}$) and (b) (for $CoSr_2(Y_{0.6}Ca_{0.4})Cu_2O_{7+\delta}$), it is clear that δ increases with increasing amount of added Ag_2O_2: $\delta \approx 0.1$ (HPO-25), 0.3 (HPO-50) and 0.3 (HPO-75) for the former system and $\delta \approx 0.2$ (HPO-12.5), 0.3 (HPO-25) and 0.4 (HPO-50) for the latter. Here note that the Rietveld refinement of the NPD data for the HPO-25 sample of the $CoSr_2(Y_{0.6}Ca_{0.4})Cu_2O_{7+\delta}$ phase (Table 2) gave an oxygen content of $\delta = 0.15$, whereas TG yielded $\delta = 0.3$. We suggest that this discrepancy might originate (besides the error bars of the two methods) from oxygen disorder in the $CoO_{1+\delta}$ charge reservoir; see further discussion in Section 3.3. Comparison among the

HPO-50 samples of the Co-1212, Co-1222 and Co-1232 phases (Fig. 3(c)) reveals that the amount of incorporated oxygen into the three phases is roughly of the same magnitude, i.e., $\delta \approx 0.3$, 0.4 and 0.4, respectively. This is quite parallel to the previous observation related to the changes in the c parameter. Thus we have succeeded in loading all the three Co-12s2 phases with a considerable and essentially equal amount of excess oxygen. Finally, we note that the onset temperatures (100–150 °C) for the oxygen evolution from the high-pressure oxygenated Co-12s2 samples are lower than those (200–350 °C) typically seen for high-T_c superconductive and related layered copper oxides [2,20]. This is considered as an indication of relatively weak bonding of the excess oxygen atoms in the $CoO_{1+\delta}$ charge reservoir of the Co-12s2 phases.

3.3. Structural changes

Fig. 4 shows the variation in the a and b lattice parameters (as refined from the XRD data) against the amount of Ag_2O_2 used in HPO treatments. Whereas the oxygen loading of the Co-12s2 phases does not significantly change the a parameter, the b parameter decreases continuously towards the a parameter, indicating symmetry change from orthorhombic to tetragonal upon full oxygenation. This may be attributed to the fact—as discussed below—that HPO breaks down the ordering of the CoO_4 tetrahedra in the $CoO_{1+\delta}$ charge reservoir.

Next we consider the average crystal structures, based on a combined refinement of SXRD and NPD data for the AS and HPO-25 samples of $CoSr_2(Y_{0.6}Ca_{0.4})Cu_2O_{7+\delta}$; see Table 2 for refined atomic coordinates. For the AS sample the orthorhombic structure model (of space group *Ima*2 originally reported by Huang et al. [5] for $CoSr_2(Y,Ca)Cu_2O_7$) was initially utilized including a split description for the oxygen atoms in $\left(x, y, \frac{1}{4}\right)$ situated in the $CoO_{1+\delta}$ layer. The main disorder appears along the short [100]. The refinements clearly indicated unequal occupancies; $n = 0.60$ for O(1) in $\left(0.413, 0.619, \frac{1}{4}\right)$, while $n = 0.40$ for O(1′) in $\left(0.627, 0.603, \frac{1}{4}\right)$. The resulting substantial spread in the Co–O(1)/O(1′) distances may result from the limitations of refinement (e.g., choice of unit cell and space group) and/or data, but may also indicate disorder in the $CoO_{1+\delta}$ layer. Such oxygen disorder would only affect the coordination polyhedra of cobalt and strontium. It should be noted that similarly distorted tetrahedral coordination and split-atom descriptions are reported for various perovskite-related oxides. However, if one disregards the tendency of unequal O(1) and O(1′) occupancies, all atomic displacements away from the more symmetric positions of space group *Imam* can probably be considered as non-significant. On the other hand, the temperature displacements for cobalt increased by a factor of two on turning from *I*2*cm* to *Imam*, which may indicate significant displacements. The *Imam* description is reported in Table 2.

High-resolution transmission-electron microscopy was thus employed to reveal the finer details. First, it was confirmed that the basic Co-12s2 structures are maintained upon HPO loading. From the HRTEM image for HPO-25 $CoSr_2(Y_{0.6}Ca_{0.4})Cu_2O_{7+\delta}$ given in Fig. 5 the ideal layer repetition of the Co-1212 structure is clearly discerned. ED patterns are shown in Fig. 6 for the AS and HPO-25 variants of $CoSr_2(Y_{0.6}Ca_{0.4})Cu_2O_{7+\delta}$ (Co-1212) with the incident electron beam along [001] and [100]. In the [001] zone-axis pattern of the AS sample, the main spots produced by the basic structure of Co-1212 are indexed on diagonals relative to the cubic perovskite mesh of dimension a_p, i.e., $a \approx b = \sqrt{2}a_p$. In addition to the main spots, weak superlattice spots that can be indexed as $\left(h, k \pm \frac{1}{4}, 0\right)$ appear, indicating double periodicity along the b-axis, i.e., $b_{super} = 2b$. Such superstructure has its

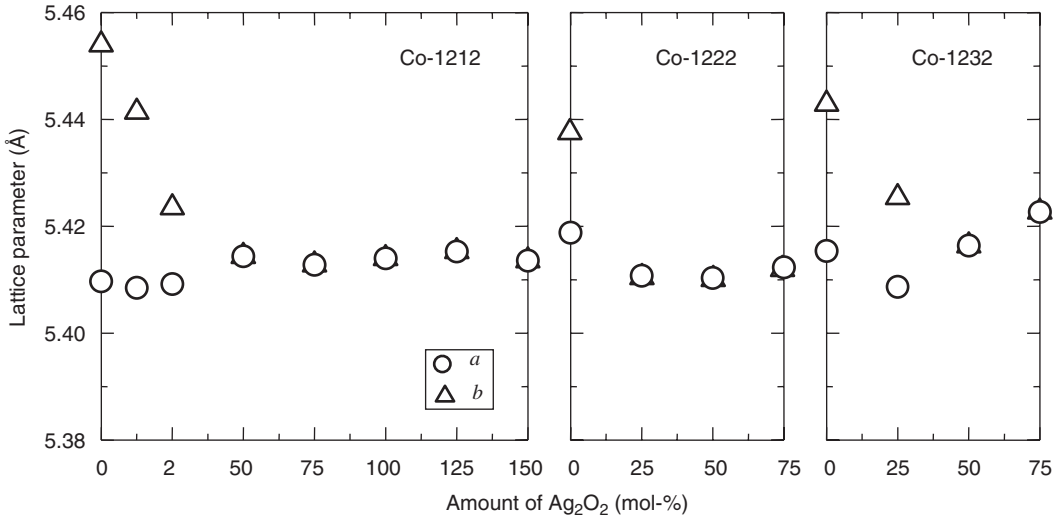

Fig. 4. Lattice parameters, a and b, plotted against the amount of Ag_2O_2 used for HPO for the three phases of $CoSr_2YCu_2O_{7+\delta}$ (Co-1212), $CoSr_2(Ce_{0.25}Y_{0.75})_2Cu_2O_{9+\delta}$ (Co-1222) and $CoSr_2(Ce_{0.67}Y_{0.33})_3Cu_2O_{11+\delta}$ (Co-1232).

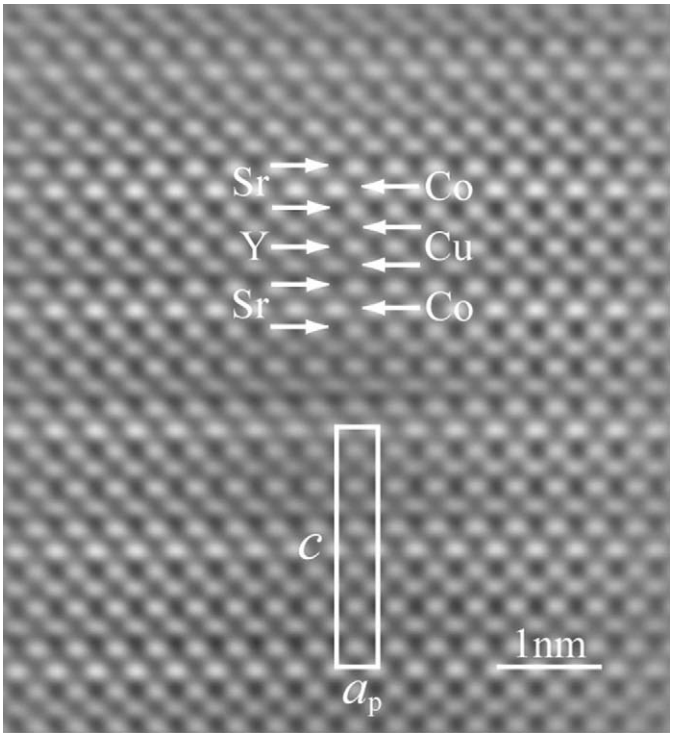

Fig. 5. HRTEM image for the HPO-25 sample of $CoSr_2(Y_{0.6}Ca_{0.4})Cu_2O_{7+\delta}$ (Co-1212).

origin in the regular ordering of two zig-zag chains of CoO_4 tetrahedra with different orientations about the *c*-axis, i.e., so-called *L* and *R* chains [4,6]. This kind of regular ordering, *–L–R–L–R–*, of the two types of chains within each charge-reservoir block has been reported earlier not only for $CoSr_2YCu_2O_7$ but also for other *M*-1212 phases with MO_4 tetrahedra (M = Ga, Al) [6]. Because an *L* chain is transferred into an *R* chain by a mirror operation, the two chain types are energetically equivalent and would hence form with equal probabilities. For the present Ca-substituted AS sample of Co-1212, $CoSr_2(Y_{0.6}Ca_{0.4})Cu_2O_{7+\delta}$ ($\delta \approx 0$), the superlattice spots are somewhat streaked along the b^* direction, suggesting that the arrangement of the *L* and *R* chains is accompanied by partial disorder, e.g., *–L–R–L–R–R–L–R–L–*. This is supported by the unequal occupancies found for the split O(1) and O(1′) atoms in the NPD refinement of the average structure in the lower symmetric *I2cm* space group, see above. In the ED patterns taken along the [100] direction, the rows of weaker spots are an indication of the *c* parameter being twice in length as compared to that of the primitive Co-1212 structure unit. In other words, the main $0\,k\,l$ reflections with k, l = even are due to the primitive Co-1212 structure, whereas the weak spots with k, l = odd are caused by a relative shift of the CoO_4 chain position between the neighboring $CoO_{1+\delta}$ charge-reservoir layers. If the weak superlattice reflections are ignored the reciprocal lattice is face centered and therefore the real lattice is body centered, which leads to a relative shift of the chain position by $\left[\frac{1}{2}\frac{1}{2}\frac{1}{2}\right]$, being in accordance with the space groups *I2cm* and *Imam* used for the average structure refinement. Judged from the ED data, the real symmetry of Co-1212 is *P2cm*. On the basis of the ED information the more complex structure model (*a*, 2*b*, 2*c*) was constructed for $CoSr_2(Y_{0.6}Ca_{0.4})Cu_2O_{7.0}$ (AS sample) and was found consistent with both the SXRD and NPD data. In this model the CoO_4-tetrahedral chains alternate as *–R–L–R–L–* along [010], and as *–L–L–R–R–* along [001].

For the HPO-25 $CoSr_2(Y_{0.6}Ca_{0.4})Cu_2O_{7+\delta}$ (Co-1212) sample the orthorhombic structure description of the corresponding AS sample with tetrahedral CoO_4 units was used as a starting point for considerations. However, it was evident that a much simpler model would be applicable. First the SXRD data were carefully analyzed. A few impurity lines were accounted for by silver (from the sample synthesis). All other reflections could be described on a tetragonal cell with $a \approx 3.82$ Å and $c \approx 11.30$ Å. This was in full agreement with the ED data where no superlattice reflections are detected in the [001] zone-axis. This was taken as an indication of either a completely disordered arrangement of the *L* and *R* chains or the disappearance of the *L*/*R* distinction due to the excess-oxygen atoms. In order to investigate in more detail whether the CoO_4 tetrahedra are less prominent as a structural motif in the HPO samples, joint refinements of both the SXRD and NPD data were carried out.

Despite the high resolution provided by the SXRD data and the sensitivity of NPD data towards oxygen displacements, no indications of symmetries lower than tetragonal were noticed. Nevertheless, initial refinements were carried out in both the *P*4/*mmm* and *Pmmm* space groups. No significant improvement was obtained on turning to the orthorhombic description. In the tetragonal description the disorder described for the $CoO_{1+\delta}$ layer of the AS sample ($\delta \approx 0$) is expected to become even more extensive for the HPO sample with $\delta > 0$. In principle, one may envisage that CoO_4 tetrahedra (of trivalent cobalt) in $CoSr_2YCu_2O_7$ could be converted into CoO_6 octahedra to form a phase of the composition of $CoSr_2YCu_2O_8$. The NPD data gave, however, only indication for a modest filling of these sites after the HPO treatment. Two sites were considered in the $CoO_{1+\delta}$ layer during Rietveld refinements: $\left(\frac{1}{2}, x, y\right)$ and $\left(\frac{1}{2}, 0, 0\right)$. The analysis of the NPD data for the HPO sample (*P*4/*mmm*) yielded an overall oxygen occupancy of these partly filled O sites (see Table 2) that corresponds to a δ value of 0.15 for HPO-25 $CoSr_2(Y_{0.6}Ca_{0.4})Cu_2O_{7+\delta}$. From the TG analysis an oxygen excess of $\delta \approx 0.3$ was estimated. It is likely that the long-range arrangement of the CoO_4 tetrahedra breaks down when additional oxygen is available within the $CoO_{1+\delta}$ layer and one may foresee numerous local coordinations. Considering the correlation in the refinement between displacement (parameters) and occupation number, one may not claim a disagreement between the NPD and the TG data. In Table 2, we present the atomic coordinates and occupation factors as refined from the NPD and/or SXRD data for both AS and HPO-25 samples of $CoSr_2(Y_{0.6}Ca_{0.4})Cu_2O_{7+\delta}$ together with

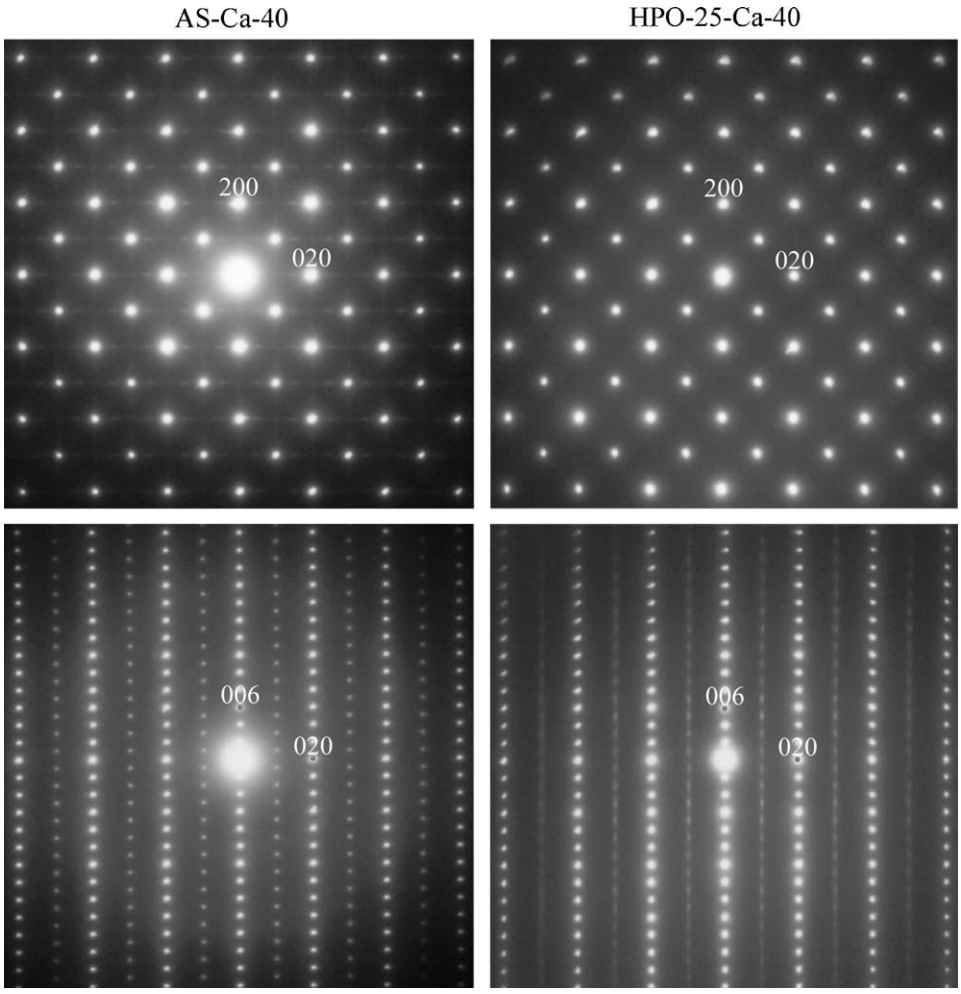

Fig. 6. ED patterns for the AS (left) and HPO-25 (right) samples of $CoSr_2(Y_{0.6}Ca_{0.4})Cu_2O_{7+\delta}$ (Co-1212) taken with the incident electron beam along the directions, [001] (upper) and [010] (lower).

those of AS samples of $CoSr_2YCu_2O_{7+\delta}$ and $CoSr_2(Ce_{0.67}Y_{0.33})_3Cu_2O_{11+\delta}$. For $CoO_{1.5}$ composition of the charge reservoir, one would expect a five-fold coordination for the Co atoms just like in, e.g., $Sr_2Mn_2O_5$ for Mn. The TG-derived oxygen content for the HPO samples suggests a distribution of tetrahedral and probably square pyramidal arrangements. One can rule out any superstructures due to ordering of such structural entities.

The ED data provided further insight into the structural details of the $CoSr_2(Y_{0.6}Ca_{0.4})Cu_2O_{7+\delta}$ HPO-25 sample. The $0\,k\,l$ reflections with k, l = odd are streaked along the c^* direction, suggesting a considerable disorder of the relative shift of the CoO_i structural entity position between neighboring $CoO_{1+\delta}$ layers, that is, a mixture of the main shift by $\left[\frac{1}{2}\frac{1}{2}\frac{1}{2}\right]$ ($\equiv A$) and a partial shift by $\left[0\,0\,\frac{1}{2}\right]$ ($\equiv B$) such as $-A-A-A-B-A-B-A-A-$.

The crystal structure of the AS sample of Co-1232 was successfully refined in space group *I2cm* based on NPD data and assuming ordered tetrahedral chain directions, however, the description was found rather equivalent to a symmetric *Imam* structure with disorder between *R* and *L* chains. Earlier ED has suggested extensive chain disorder in Co-1232 [4]. This supports the *Imam* description given in Table 3. Note, however, that like Co-1212, also the symmetric *Imam* description for Co-1232 leads to enhanced thermal displacements for cobalt that may indicate symmetry lowering. Since the Co-1212 phase is known to be the Co-12*s*2 phase with the highest degree of CoO_4-chain ordering (for AS samples) [4], we believe that the presently observed destruction of chain ordering in Co-1212 upon HPO treatment will also occur for both Co-1222 and Co-1232. However, no ND data were collected for the HPO samples of these phases.

3.4. Hole doping and superconductivity

All present AS samples were found non-superconductive in accordance with previous reports on the Co-12*s*2 phases [3–10]. For the HPO samples of $CoSr_2YCu_2O_{7+\delta}$ superconductivity appeared when the amount of Ag_2O_2 used for the HPO treatment was 25 mol% or larger, whereas the higher members of the Co-12*s*2 homologous series remained non-superconductive despite the successful oxygen loading. To elucidate the reason for that, the changes

Table 3
Atomic coordinates for $CoSr_2(Ce_{0.67}Y_{0.33})_3Cu_2O_{11.0}$ at 8 and 298 K as derived from Rietveld refinements of NPD data

	AS 298 K	AS 8 K
Space group	*Imam*	*Imam*
Z	4	4
a (Å)	5.4183(2)	5.4092(2)
b (Å)	5.4447(2)	5.4356(2)
c (Å)	33.605(1)	33.519(1)
V (Å^3)	991.38(7)	985.53(7)
Y1/Ce1		
x	0	0
y	0.5	0.5
z	0.5	0.5
Uiso	0.26(5)	0.18(5)
Y2/Ce2		
x	0	0
y	0.003(2)	0.004(2)
z	0.4231(1)	0.4232(1)
Uiso	0.26(5)	0.18(5)
Sr		
x	0	0
y	0.004(2)	0.003(2)
z	0.3179(1)	0.3179(1)
Uiso	0.74(9)	0.28(9)
Co		
x	0	0
y	0.459(6)	0.451(6)
z	0.75	0.75
Uiso	2.5(6)	2.2(6)
Cu		
x	0.5	0.5
y	0.004(2)	0.003(2)
z	0.3697(1)	0.3695(1)
Uiso	0.32(7)	0.20(7)
O(1)		
x	0.75	0.75
y	0.25	0.25
z	0.3756(3)	0.3756(3)
Uiso	0.40(4)	0.05(4)
O(2)		
x	0.25	0.25
y	0.75	0.75
z	0.3756(3)	0.3756(3)
Uiso	0.40(4)	0.05(4)
O(3)		
x	0.381(3)	0.391(3)
y	0.600(3)	0.613(3)
z	0.25	0.25
Uiso	0.40(4)	0.05(4)
O(4)		
x	0	0
y	0.471(1)	0.474(1)
z	0.301(1)	0.301(1)
Uiso	0.40(4)	0.05(4)
O(5)		
x	0.75	0.75
y	0.25	0.25
z	0.458(2)	0.458(2)
Uiso	0.40(4)	0.05(4)
O(6)		
x	0.25	0.25
y	0.75	0.75
z	0.461(2)	0.461(2)
Uiso	0.40(4)	0.05(4)

Calculated standard deviations are in parentheses. O(3) site half filled due to chain disorder, see text.

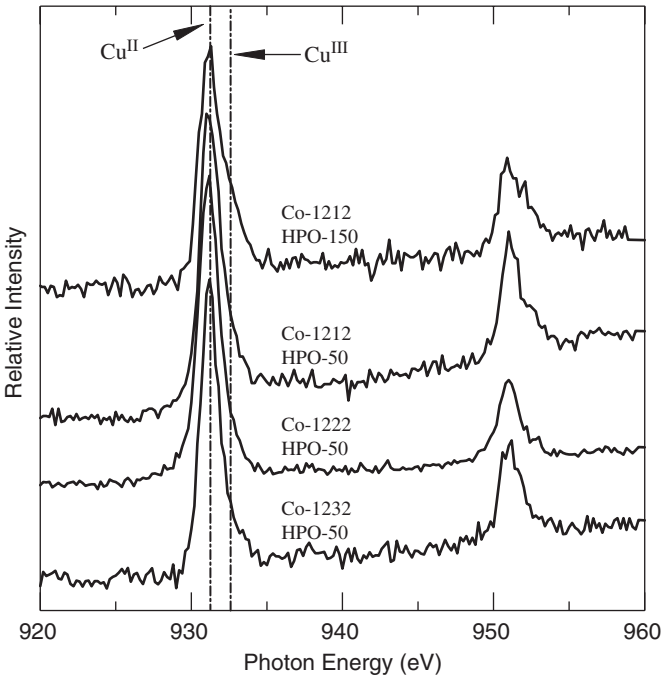

Fig. 7. Cu L_3-edge XANES spectra for some representative samples.

in the valence state of copper or the hole-doping level of the CuO_2 plane were followed by means of Cu *L*-edge XANES spectroscopy. In Fig. 7 shown are representative spectra for the present samples. The valence of copper, *V*(Cu), was calculated from each fitted spectrum as described in Section 2.3. For the AS samples of all the three phases, $CoSr_2YCu_2O_{7+\delta}$, $CoSr_2(Ce_{0.25}Y_{0.75})_2Cu_2O_{9+\delta}$ and $CoSr_2(Ce_{0.67}Y_{0.33})_3Cu_2O_{11+\delta}$, *V*(Cu) was found to be very low, i.e., 2.00 ($s = 1$), 2.05 ($s = 2$) and 2.06 ($s = 3$), explaining the absence of superconductivity in these samples. We further use the *V*(Cu) values to calculate the valence of cobalt, *V*(Co), in the AS samples. This is possible since the precise oxygen content has been determined for the AS samples, i.e., they were shown to be essentially oxygen stoichiometric. Using $\delta = 0$, *V*(Co) is calculated to be 3.00 ($s = 1$), 3.40 ($s = 2$) and 2.87 ($s = 3$), on the assumption that $V(Sr) = 2$, $V(Ce) = 4$ and $V(Y) = 3$. It thus seems that *V*(Co) is in the vicinity of 3 but not necessarily exactly the same for the three phases even though Co possesses (at

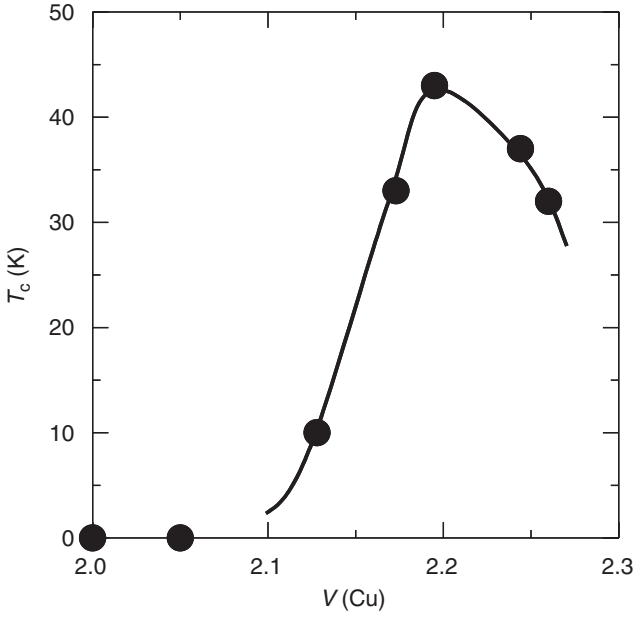

Fig. 8. T_c versus V(Cu) for $CoSr_2YCu_2O_{7+\delta}$ of the Co-1212 phase with different oxygen contents as obtained through HPO using different amounts of Ag_2O_2.

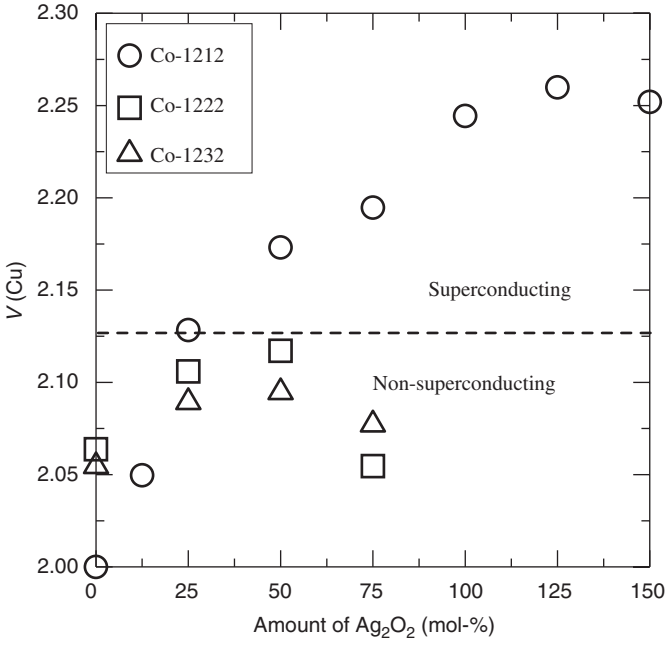

Fig. 9. V(Cu) versus amount of Ag_2O_2 used in HPO for the three phases of $CoSr_2YCu_2O_{7+\delta}$ (Co-1212), $CoSr_2(Ce_{0.25}Y_{0.75})_2Cu_2O_{9+\delta}$ (Co-1222) and $CoSr_2(Ce_{0.67}Y_{0.33})_3Cu_2O_{11+\delta}$ (Co-1232).

least qualitatively) equivalent coordination polyhedra (= tetrahedral) in the AS samples of all the members of the Co-12s2 homologous series.

For $CoSr_2YCu_2O_{7+\delta}$ (Co-1212), V(Cu) increases monotonically as the amount of Ag_2O_2 used as an oxygen source was increased up to ~100 mol%. Samples with $V(Cu) \geqslant 2.13$ are superconductive and the "optimum doping level" corresponding to the highest T_c value of 43 K is found about $V(Cu) = 2.19$ (see Fig. 8). On the other hand, the Co-1222 and Co-1232 phases did not show any sign of superconductivity even after the HPO treatments. A plausible reason is seen from Fig. 9 where the value of V(Cu) is plotted for the Co-12s2 series against the amount of Ag_2O_2 added. The maximum values of V(Cu) as reached for Co-1222 (2.09) and Co-1232 (2.12) are somewhat lower than the "superconductivity-onset" V(Cu) value of 2.13 for Co-1212. Hence we believe that the absence of superconductivity in our HPO samples of the Co-1222 and Co-1232 phases is due to the too low hole-doping level rather than, e.g., weakened coupling between the CuO_2 planes [21]. From Fig. 9, it seems probable that if more holes could be doped into the CuO_2 plane superconductivity would most likely appear also in Co-1222 and Co-1232. On the other hand, oxygen loading to a larger extent than achieved in the present work seems not possible, at least by means of the HPO technique employed. Therefore it is necessary to find another technique to induce more holes in the CuO_2 planes of the Co-1222 and Co-1232 phases. In future works the possibilities provided by aliovalent cation substitutions should be investigated in detail.

In the $CoSr_2YCu_2O_{7+\delta}$ (Co-1212) phase, the trivalent yttrium site can be occupied by divalent Ca up to ~40%

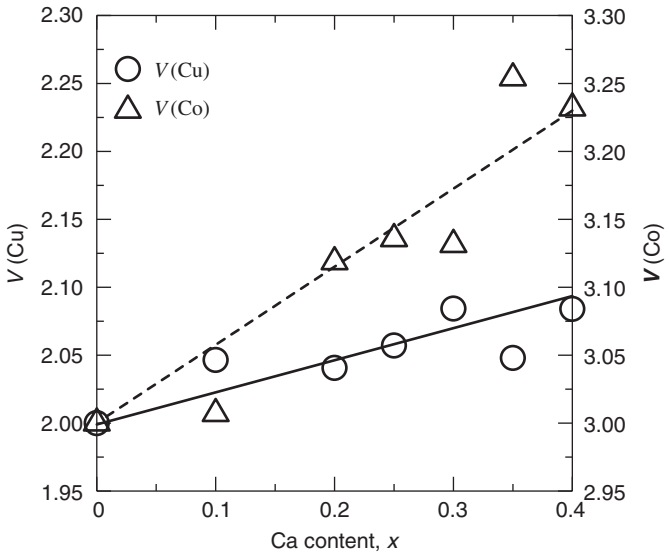

Fig. 10. V(Cu) and V(Co) for the AS samples of $CoSr_2(Y_{1-x}Ca_x)Cu_2O_{7.0}$ with increasing Ca content, x.

[5,10]. Upon aliovalent Ca^{II}-for-Y^{III} substitution the oxygen content of the AS samples remains constant, i.e., at $\delta = 0.00(3)$ [10]. Thus for these samples the pure divalent-for-trivalent cation substitution effect can be investigated. From the XANES data it is found that V(Cu) in $CoSr_2(Y_{1-x}Ca_x)Cu_2O_{7.0}$ remains below 2.08 even for the sample most heavily ($x = 0.4$) substituted with Ca. In Fig. 10, the value of V(Cu) is plotted against Ca content, x. Also shown are the values for V(Co) as calculated from

those of δ (= 0) and V(Cu). It is seen that the holes created through Ca^{II}-for-Y^{III} substitution are not efficiently directed into the CuO_2 plane, but rather trapped on Co in the charge reservoir: whereas the value of V(Cu) is increased up to 2.08 only, V(Co) reaches a value of 3.23 for $x = 0.4$. Note that for the non-doped $x = 0$ parent, V(Cu) = 2.00 and V(Co) = 3.00.

In the same way as for the Ca-free $CoSr_2YCu_2O_{7+\delta}$ system, oxygen loading induces superconductivity in Ca-substituted $CoSr_2(Y_{1-x}Ca_x)Cu_2O_{7+\delta}$ samples, and the T_c value depends on the amount of Ag_2O_2 used in the HPO treatment. In Fig. 11 plotted is the value of T_c against V(Cu) for three sample series with different Ca contents of $x = 0$, 0.2 and 0.4. Here two interesting observations can be made by comparing the T_c values of the three sample series. Firstly, at a fixed V(Cu) value the value of T_c depends on the Ca content x. Secondly, also the maximum value of T_c is a function of x, being 43 K for $x = 0$ (HPO-75), 47 K for $x = 0.2$ (HPO-50) and 32 K for $x = 0.4$ (HPO-25). Parallel observations were previously reported for the related Cu-1212 phase using differently Ca-substituted/O-doped samples of $Cu(Ba_{0.8}Sr_{0.2})_2(Yb_{1-x}Ca_x)Cu_2O_{6+\delta}$ [22–24]. In $Cu(Ba_{0.8}Sr_{0.2})_2(Yb_{1-x}Ca_x)Cu_2O_{6+\delta}$ the maximum T_c value was found at 82 K for $x = 0$ ($\delta = 0.96$), 80 K for $x = 0.05$ ($\delta = 6.80$) and 79 K for $x = 0.35$ ($\delta = 6.52$) [22]. Thus both in Co-1212 and Cu-1212 aliovalent Ca^{II}-for-R^{III} substitution contributes to the hole doping in such a way that the higher the Ca content is, the less excess oxygen is needed to reach the maximum T_c value. Furthermore, the present results for Co-1212 provide us with additional evidence for our previous conclusion [23,24] that even within the same phase, the value of T_c is controlled—besides the CuO_2-plane hole concentration—by other factors too.

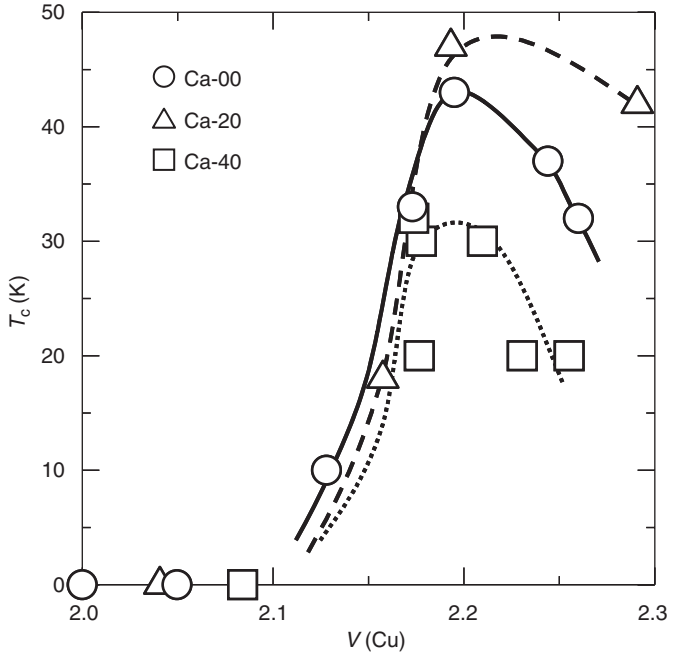

Fig. 11. V(Cu) versus x for the three series of AS samples of $CoSr_2(Y_{1-x}Ca_x)Cu_2O_{7.0}$ with $x = 0.0$, 0.2 and 0.4.

Table 4
Room-temperature Cu–O bond lengths (in Å) and the calculated BVS(Cu) values for Co-1212 ($CoSr_2(Y_{1-x}Ca_x)Cu_2O_{7+\delta}$: $x = 0$, AS and $x = 0.4$, AS and HPO-25) and Co-1232 ($CoSr_2(Ce_{0.67}Y_{0.33})_3Cu_2O_{11.0}$) samples calculated on the basis of results from Rietveld refinements of NPD and SXRD diffraction data, Tables 2 and 3

	Co-1212 $x = 0.0$ AS	Co-1212 $x = 0.4$ AS	Co-1212 $x = 0.4$ HPO-25	Co-1232 AS
$Cu–O_{api}$	2.348	2.353	2.196	2.311
$Cu–O_a$	1.934 × 2	1.921 × 2	1.912 × 4	1.915 × 2
$Cu–O_b$	1.934 × 2	1.930 × 2		1.946 × 2
BVS(Cu)	2.17	2.23	2.38	2.2

Finally we note that the V(Cu) values determined for Co-12s2 samples from the Cu L-edge XANES data are highly parallel to those estimated for the same samples through BVS calculations (Table 4) whenever the comparison is possible. In general, although the BVS(Cu) values [25] are somewhat higher than the corresponding V(Cu)'s, the conclusions are essentially the same. For the non-doped (AS) $CoSr_2YCu_2O_{7.0}$ of the Co-1212 phase BVS(Cu) = 2.17 (V(Cu) = 2.00). Aliovalent Ca^{II}-for-Y^{III} substitution increases the valence state of copper slightly but not enough to induce superconductivity for the AS $CoSr_2(Y_{0.6}Ca_{0.4})Cu_2O_{7.0}$ sample, i.e., BVS(Cu) = 2.23 (V(Cu) = 2.08). For the oxygenated HPO-25 $CoSr_2(Y_{0.6}Ca_{0.4})Cu_2O_{7+\delta}$ sample the BVS(Cu) value reaches 2.38 (V(Cu) = 2.17). Finally, the valence state of copper is slightly higher in AS Co-1232 (BVS(Cu) = 2.20, V(Cu) = 2.06) than in the Ca-free AS Co-1212 (BVS(Cu) = 2.17, V(Cu) = 2.00).

3.5. Magnetic properties

The 8 K neutron diffraction data show one clear additional magnetic peak for the AS samples ($\delta \approx 0$) of the $CoSr_2(Y_{0.6}Ca_{0.4})Cu_2O_{7+\delta}$ (Co-1212) and $CoSr_2(Ce_{0.67}Y_{0.33})_3Cu_2O_{11+\delta}$ (Co-1232) phases. In both cases, the somewhat broad magnetic peak around $d = 5.3$ Å corresponds to (100)/(010) and/or (101)/(011), see the difference plot for NPD data collected at 8 and 298 K for the latter Co-1232 phase in Fig. 12. In cobalt oxides like $La_3Co_3O_8$ and $La_2Co_2O_5$ with CoO_4-tetrahedral chains, antiferromagnetic (AFM) order is typically observed [26]. For these $La_nCo_nO_{3n-1}$ and related phases, the ordering temperature (T_N) is lowered upon increasing the fraction of Co^{III} octahedral entities with respect to Co^{II} tetrahedral entities. A simple model for Co-1212 and Co-1232 assuming a similar AFM coupling within the CoO_4-tetrahedral chains along [110] and AFM coupling along [001] gave a reasonable fit to the observations of the single major AFM peak. The refinements indicate that the magnetic structure at 8 K has its major component along [001], with magnetic moments $\mu_{AFM} = 2.5(3)\mu_B$. Although this does

not prove that copper is inert in the magnetic ordering process, it is rather a statement that the observations can be explained on the basis of the cobalt substructure alone. It should be noted that no proof for AFM ordering was found in the NPD patterns for the HPO samples.

The magnetic susceptibility (χ) versus temperature (T) data for AS and HPO samples of Co-1212 given in Fig. 13(a) have several characteristics. First, the $\chi(T)$ curve for the AS sample shows deviation between ZFC and FC branches around 200 K. Since the NPD experiment proved long-range AFM order at 8 K, one could suggest that this reflects T_N. On the other hand, it may also indicate onset of strong intrachain or interchain interactions within the various $CoO_{1+\delta}$-stacking planes, and that complete 3D-order first occurs at a lower temperature, e.g., at the kink seen around 50 K. Such a low ordering temperature seems plausible regarding the long interplane separation of about 5.7 Å. Similar features are evident for the HPO-25 sample. For the other HPO samples, the susceptibility shows onset of superconductivity below some 40 K. For the HPO-100, HPO-125 and HPO-150 samples, a clear feature is seen in $\chi(T)$ about 75–90 K. This may reflect onset of AFM interactions, within or between chains, or even on a long range, which indeed can be expected from crystal structure arguments since oxygen incorporation in the $CoO_{1+\delta}$ layer may enhance interchain interactions. It is, however, also possible that the feature originates from an unidentified impurity, see the Section 3.1.

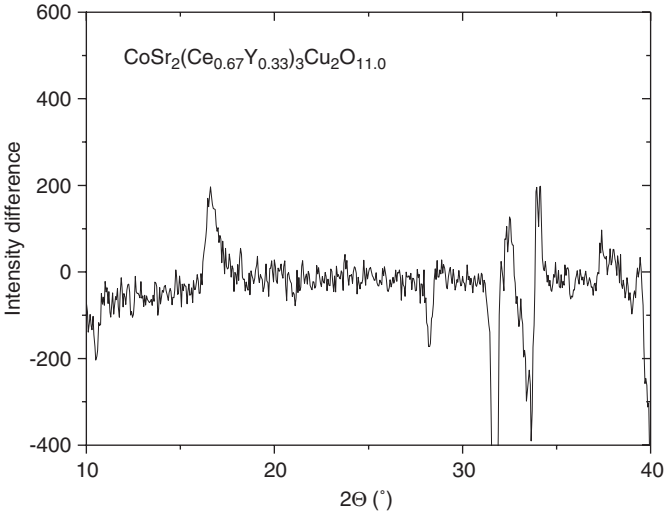

Fig. 12. Difference plot for NPD data collected at 8 and 298 K for the AS $CoSr_2(Ce_{0.67}Y_{0.33})_3Cu_2O_{11.0}$ sample of the Co-1232 phase showing a magnetic peak at $2\theta \approx 16.5^\circ$.

The $\chi - T$ data for Co-1222 and Co-1232 are displayed in Figs. 13(b) and (c), respectively, showing features essentially similar to those for Co-1212. (The strongly enhanced feature seen for the HPO Co-1232 samples in Fig. 13(c) is presumably not intrinsic, but due to small impurities of $SrCoO_y$ phases.)

4. Conclusions

The three first members ($s = 1, 2, 3$) of the Co-12s2 homologous series of multi-layered copper oxides that

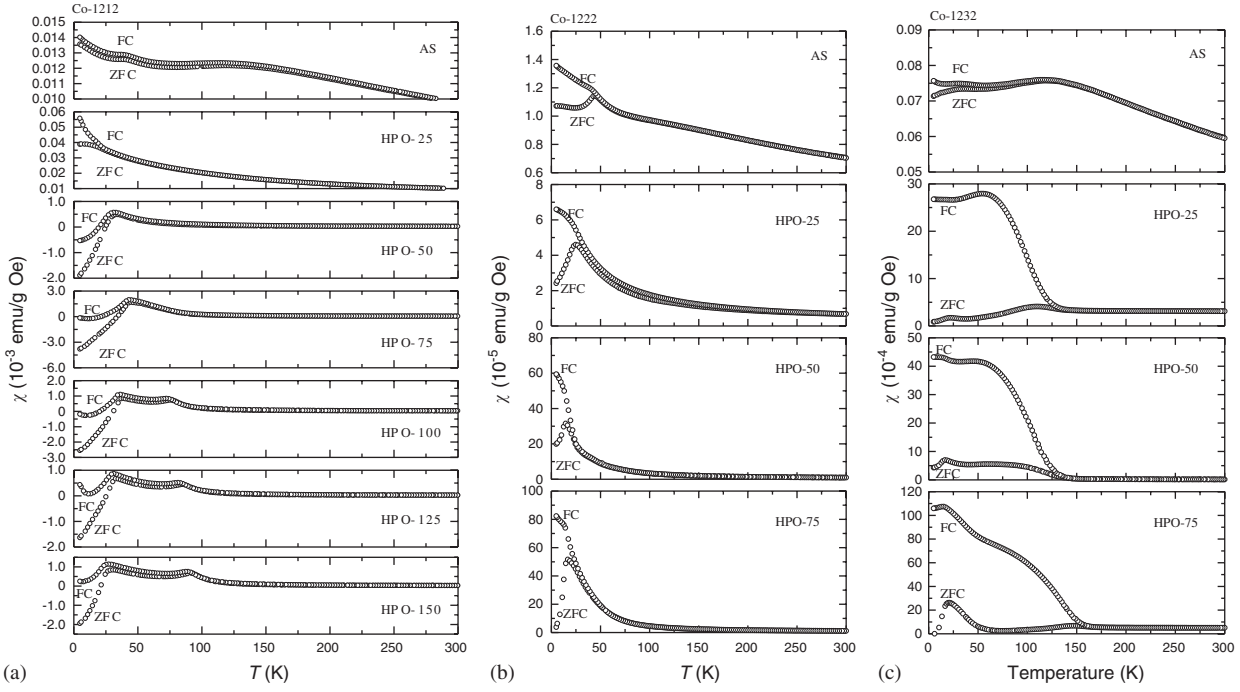

Fig. 13. Magnetization (χ versus T) for AS and HPO samples of (a) $CoSr_2YCu_2O_{7+\delta}$ (Co-1212), (b) $CoSr_2(Ce_{0.25}Y_{0.75})_2Cu_2O_{9+\delta}$ (Co-1222), and (c) $CoSr_2(Ce_{0.67}Y_{0.33})_3Cu_2O_{11+\delta}$ (Co-1232).

differ from each other only in terms of the (Ce,Y,Ca)–$[O_2$–(Ce,Y)$]_{s-1}$ layer block between two identical CuO_2 planes have been gradually doped with holes through high-pressure oxygenation (HPO). HRTEM and ED analyses together with synchrotron X-ray and neutron powder diffraction data reveal that as a consequence of the HPO the charge-reservoir CoO_4-tetrahedra chains get broken and the lattice symmetry transforms from orthorhombic to tetragonal. Oxygen contents are estimated for the samples on the bases of wet-chemical and thermogravimetric analyses. The valence state of copper in the CuO_2 plane is determined from Cu *L*-edge XANES spectra and additionally estimated through BVS calculations based on the crystal structure data. It is found that the positive charge induced by oxygen loading is not completely directed into the CuO_2 planes but is rather effectively trapped by the charge-reservoir Co atoms. The same applies in the case of Co-1212 when it is doped—instead of by HPO—through aliovalent Ca^{II}-for-Y^{III} substitution. For Co-1212 ($CoSr_2YCu_2O_{7+\delta}$) superconductivity appears in the samples with the copper valence at 2.13 or higher, whereas for Co-1222 ($CoSr_2(Ce_{0.25}Y_{0.75})_2Cu_2O_{9+\delta}$) and Co-1232 ($CoSr_2(Ce_{0.67}Y_{0.33})_3Cu_2O_{11+\delta}$) the CuO_2-plane hole concentration does not increase high enough to induce superconductivity in these phases.

Acknowledgments

This work was supported by Grants-in-aid for Scientific Research (Nos. 15206002 and 15206071) from the Japan Society for the Promotion of Science, and the Nanotechnology Support Project of the MEXT, Japan. Prof. Y. Moritomo and Dr. K. Kato are thanked for the synchrotron-radiation X-ray powder diffraction experiments which were performed at the Spring-8 BL02B2 beamline with approval of the Japan Synchrotron Radiation Research Institute (JASRI). The present work was primarily accomplished during the Visiting Professorship of H.F. at Materials and Structures Laboratory, Tokyo Institute of Technology. H.F. acknowledges project support by the Research Council of Norway, Grant. No. 158518/431 (NANOMAT).

References

[1] T. Wada, A. Ichinose, H. Yamauchi, S. Tanaka, J. Ceram. Soc. Jpn. Int. Ed. 99 (1991) 420.
[2] M. Karppinen, H. Yamauchi, Mater. Sci. Eng. R 26 (1999) 51.
[3] M. Karppinen, V.P.S. Awana, Y. Morita, H. Yamauchi, Physica C 392–396 (2003) 82.
[4] T. Nagai, V.P.S. Awana, E. Takayama-Muromachi, A. Yamazaki, M. Karppinen, H. Yamauchi, S.K. Malik, W.B. Yelon, Y. Matsui, J. Solid State Chem. 176 (2003) 213.
[5] Q. Huang, R.J. Cava, A. Santoro, J.J. Krajewski, W.F. Peck, Physica C 193 (1992) 196.
[6] T. Krekels, O. Milat, G. van Tendeloo, S. Amelinckx, T.G.N. Babu, A.J. Wright, C. Greaves, J. Solid State Chem. 105 (1993) 313.
[7] V.P.S. Awana, S.K. Malik, W.B. Yelon, M. Karppinen, H. Yamauchi, Physica C 378–381 (2002) 155.
[8] R.J. Cava, H.W. Zandberger, J.J. Krajewski, W.F. Peck Jr., B. Hessen, R.B. Van Dover, S.-W. Cheong, Physica C 198 (1992) 27.
[9] V.P.S. Awana, A. Gupta, H. Kishan, S.K. Malik, W.B. Yelon, J. Lindén, M. Karppinen, H. Yamauchi, D.C. Kundaliya, J. Appl. Phys. 95 (2004) 6690.
[10] Y. Morita, H. Yamauchi, M. Karppinen, Solid State Comm. 127 (2003) 493.
[11] The cation stoichiometries used are based on our preliminary work on searching for the single-phase regions for the Co-12*s*2 phases. It was found that the solubility limit of Ca at the Y site in Co-1212 is around 40%, and that the Ce:Y ratios in the Co-1222 and Co-1232 phases can not deviate much from the ratios selected here.
[12] M. Karppinen, M. Matvejeff, K. Salomäki, H. Yamauchi, J. Mater. Chem. 12 (2002) 1761.
[13] J.M. Chen, R.S. Liu, W.Y. Liang, Phys. Rev. B 54 (1996) 12587.
[14] M. Karppinen, H. Yamauchi, Y. Morita, M. Kitabatake, T. Motohashi, R.S. Liu, J.M. Lee, J.M. Chen, J. Solid State Chem. 177 (2004) 1037.
[15] A. Bianconi, M. DeSantis, A. Di Ciccio, A.M. Flank, A. Fronk, A. Fontaine, P. Legarde, H.K. Yoshida, A. Kotani, A. Marcelli, Phys. Rev. B 38 (1988) 7196.
[16] N. Nücker, E. Pellegrin, P. Schweiss, J. Fink, S.L. Molodtsov, C.T. Simmons, G. Kaindl, W. Frentrup, A. Erb, G. Müller-Vogt, Phys. Rev. B 51 (1995) 8529.
[17] A.C. Larson, R.B. Von Dreele, Program GSAS, General Structure Analysis System, LANSCE, MS-H 805, Los Alamos National Laboratory, Los Alamos, NM 87545, USA
[18] J. Rodriguez-Carvajal, FULLPROF Computer Program, Version 2.80, LLB, Saclay, 2004.
[19] N.E. Brese, M. O'Keeffe, Acta Crystallogr. 47 (1991) 192.
[20] M. Karppinen, H. Yamauchi, Oxygen engineering for functional oxide materials, in: A.V. Narlikar (Ed.), International Book Series: Studies of High Temperature Superconductors, vol. 37, Nova Science Publishers, New York, 2001, pp. 109–143.
[21] J.M. Chen, S.C. Chang, R.S. Liu, J.M. Lee, M. Park, J.H. Choy, Phys. Rev. B 71 (2005) 94501.
[22] K. Fujinami, M. Karppinen, H. Yamauchi, Physica C 300 (1998) 17.
[23] M. Karppinen, H. Yamauchi, K. Fujinami, T. Nakane, K. Peitola, H. Rundlöf, R. Tellgren, Phys. Rev. B 60 (1999) 4378.
[24] M. Karppinen, H. Yamauchi, T. Nakane, K. Fujinami, K. Lehmus, P. Nachimuthu, R.S. Liu, J.M. Chen, J. Solid State Chem. 166 (2002) 229.
[25] The absolute values of BVS are not very accurate, but within a sample/homologous series relative values should be meaningful.
[26] O.H. Hansteen, H. Fjellvåg, B.C. Hauback, J. Mater. Chem. 8 (1998) 2081.